Chinese Journal of
POLYMER SCIENCE

RESEARCH ARTICLE

https://doi.org/10.1007/s10118-023-2997-0
Chinese J. Polym. Sci. **2023**, *41*, 1868–1878

Design of Tough, yet Strong, Heat-resistant PLA/PBAT Blends with Reconfigurable Shape Memory Behavior by Engineering Exchangeable Covalent Crosslinks

Xiao-Wen Zhou, Jing Huang*, Xu-Hui Zhang, Ting Li, Yang Wang, Shi-Bo Wang, Bi-Hua Xia, and Wei-Fu Dong*

The Key Laboratory of Synthetic and Biological Colloids, Ministry of Education, School of Chemical and Material Engineering, Jiangnan University, Wuxi 214122, China

Electronic Supplementary Information

Abstract Polylactide (PLA) has often been blended with biodegradable poly(butylene adipate-*co*-terephthalate) (PBAT) to improve its toughness. However, the strength and heat resistance of PLA are always sacrificed. Herein, exchangeable hydroxyl-ester crosslinks are constructed in PLA/PBAT blends by successively introducing a tertiary amine-containing polyol, bis-(2-hydroxyethyl)amino-tris (hydroxymethyl)methane (BTM) and 4,4′-diphenylmethane diisocyanate (MDI) *via* reactive blending. BTM can react with both PLA and PBAT by transesterification, generating PLA or PBAT chains with terminal or pendant hydroxyl groups, which can then react with MDI to form networks. With internal catalysis of tertiary amine moiety in BTM, transesterification between the residual hydroxyl groups and ester bonds can occur at high temperatures, endowing the PLA/PBAT network with vitrimeric properties. Owning to the transesterification and chain extension reactions with MDI between PLA and PBAT, the interfacial adhesion is greatly improved. As a result of the excellent interfacial adhesion and the network structure, the prepared PLA/PBAT blends show greatly enhanced heat resistance and toughness (more than 40 times that of PLA) while maintaining high stiffness comparable to PLA. Furthermore, the prepared PLA/PBAT blends exhibit promising reconfigurable shape memory behavior. The present work provides a new and facile way to achieve high-performance and functional biodegradable polymeric materials.

Keywords Polylactide; Dynamic covalent bonds; Strengthening and toughening; Heat resistance; Shape memory

Citation: Zhou, X. W.; Huang, J.; Zhang, X. H.; Li, T.; Wang, Y.; Wang, S. B.; Xia, B. H.; Dong, W. F. Design of tough, yet strong, heat-resistant PLA/PBAT blends with reconfigurable shape memory behavior by engineering exchangeable covalent crosslinks. *Chinese J. Polym. Sci.* **2023**, *41*, 1868–1878.

INTRODUCTION

Plastics have indispensable applications in daily life, but plastics at their end of life have brought about serious environmental problems. It is estimated that global plastic waste will reach about 12 billion tons by 2050.[1] The pandemic of Covid-19 makes the situation worse due to the huge consumption of facemasks and gloves.[2] To address plastic pollution, many efforts have been made to develop biodegradable plastics alternatives, which is considered as one of the most promising solutions.[3,4] Among biodegradable plastics, polylactide (PLA) has seen significant commercial growth because of its renewable and low-cost nature, high mechanical strength and good biocompatibility.[5,6] However, the brittleness and poor resistance to heat deformation of PLA prevent it from being applied widely in advanced engineering fields such as automotive industries, electronics, and biomedical devices.[7,8]

* Corresponding authors, E-mail: jinghuang@jiangnan.edu.cn (J.H.)
E-mail: wfdong@jiangnan.edu.cn (W.F.D.)

Received March 21, 2023; Accepted May 5, 2023; Published online June 15, 2023

To toughen PLA, it is often blended with flexible polymers,[9–11] especially with biodegradable polyesters, such as poly(butylene adipate-*co*-terephthalate) (PBAT),[12–14] poly(propylene carbonate) (PPC)[15,16] and polycaprolactone (PCL),[17,18] which can maintain its biodegradability. In this way, compatibilizers are usually needed due to the poor miscibility between different polyesters. Additionally, the stiffness and heat resistance are often compromised. In this regard, additional annealing treatment or nucleating agents can be used to improve the crystallinity of PLA, and thus improve the stiffness and heat resistance of the blends,[19–21] but it usually still needs an annealing process to achieve a satisfying crystallinity, which would increase the complexity of processing and defective rate of the products. Apart from promoting crystallinity, crosslinking is another effective way to improve the stiffness and the heat resistance of a linear polymeric material including PLA.[22,23] However, permanent crosslinks would make the material lose its thermoplasticity, which prevents the material from being fabricated by a straightforward melting blending and hot pressing, thus a post-curing process is often necessary, for example crosslink-

ing by radiation.[24] Moreover, once the material is crosslinked, it cannot be reshaped and reprocessed, causing recycling problems shared with thermosets.

A novel kind of polymer material crosslinked with exchangeable covalent bonds, named vitrimers, have received much attention in the past decade, as they can be reprocessed like thermoplastics although they are permanently crosslinked.[25,26] The unique properties of vitrimers are enabled by the rearrangement of network topology resulting from the exchange reactions between the covalent bonds at high temperatures. The concept of vitrimers has been introduced to commercially available thermoplastics including polystyrene,[27] polymethyl methacrylate,[27,28] polyethylene,[27,29] polypropylene,[30] poly(butylene terephthalate),[31] and polyethylene terephthalate,[32] to improve their mechanical properties and resistance to thermal and solvents deformation, while maintaining their thermal processability. PLA vitrimers have also been reported due to their bio-based and biodegradable nature.[33–35] Hillmyer *et al.* first demonstrated a PLA vitrimer, which was prepared by using methylenediphenyl diisocyanate to crosslink a synthesized hydroxyl-terminated star-shaped PLA. The residual hydroxyl groups in the system can react with ester groups in the PLA backbone *via* transesterification under the catalysis of $Sn(Oct)_2$ at high temperatures, thus endowing the material with vitrimeric properties.[33] Very recently, Bao *et al.* fabricated a PLA vitrimer by two-step alcoholysis and transesterification *via* reactive processing in order to improve the melt strength of PLA and as such for better foaming performance. However, the obtained PLA vitrimer are quite brittle with a tensile strain of about 1% and a tensile strength of around 29 MPa.[35]

In this study, we incorporated exchangeable covalent bonds into commercial PLA/PBAT blends by reactive blending. PLA/PBAT was first blended with a tertiary amine-containing polyol, bis-(2-hydroxyethyl)amino-tris (hydroxymethyl)methane (BTM), which can inset in PLA or PBAT chains by internally catalyzed transesterification, forming PLA or PBAT chains with terminal or pendant hydroxyl groups. Afterward, 4,4′-diphenylmethane diisocyanate (MDI) was added to react with the hydroxyl groups and connect the polymer chains as a crosslinking agent. At last, PLA/PBAT networks were achieved (Fig. 1). During the reactive blending, internal catalyzed transesterification occurs between residual hydroxyl groups and ester groups in PLA or PBAT backbone, thus the prepared PLA/PBAT networks possess vitrimeric properties, which can be subject to melt blending and subsequent hot pressing. Due to the confinement of the network structure, the prepared PLA/PBAT networks shows greatly improved resistance to heat deformation. Importantly, because of the interfacial transesterification and chain extension reactions between PLA and PBAT, the vitrimeric PLA/PBAT blends present excellent interfacial adhesion. As a result, both the mechanical strength and toughness of the blends are significantly improved, showing a good balance between stiffness and toughness. Moreover, the resultant PLA/PBAT blends present promising reconfigurable shape memory behavior.

EXPERIMENTAL

Materials

A commercially available PLA (4032D) was purchased from Nature Works LLC (Minnetonka, MN). It has a density of 1.24 g/cm^3 and a weight-average molecular weight (M_w) of 2.07×10^5 g/mol. The melting point (T_m) of PLA is 159.2 °C. PBAT with a density of 1.22 g/cm^3, was supplied by Kanghui New Material of Hengli Petrochemical Co., Ltd. (China). The melting point (T_m) of PBAT is 116 °C. The antioxidant (Irganox 1076) was supplied by

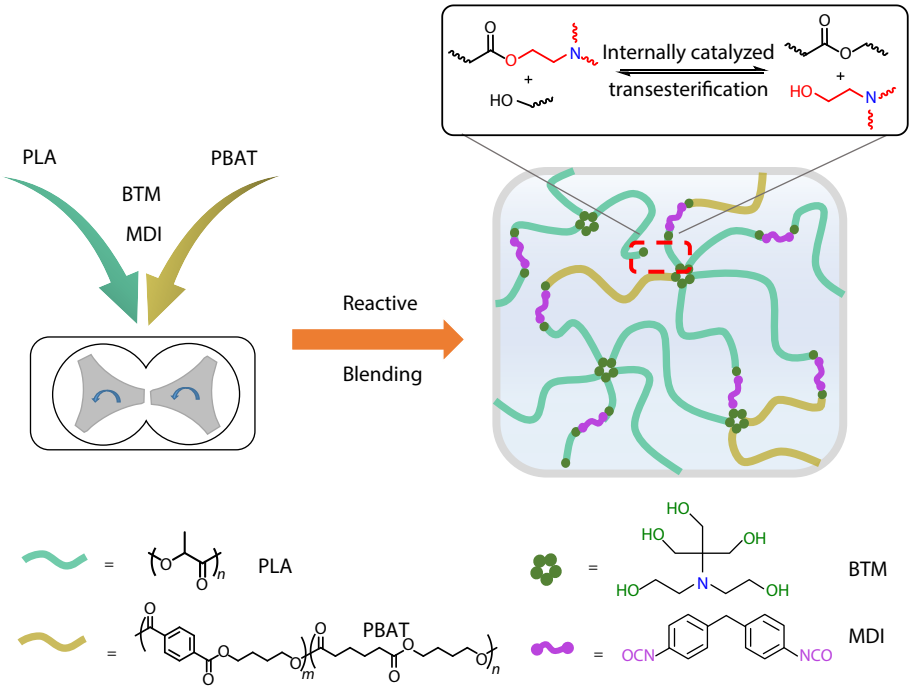

Fig. 1 Schematical illustration of the preparation of vitrimeric PLA/PBAT blends based on transesterification by reactive blending.

https://doi.org/10.1007/s10118-023-2997-0

BASF. 2,2-Bis(hydroxymethyl)-2,2′,2″-nitrilotriethanol (BTM, 99%) and 4,4′-methylene bis (phenyl isocyanate) (MDI, 98%) were purchased from Macklin Inc.

Preparation of the Vitrimeric PLA/PBAT Blends

PLA and PBAT pellets were dried at 70 °C overnight in a vacuum oven to remove water and cooled to room temperature naturally before use. PLA/PBAT and the additives were melt-blended in a Haake internal mixer at 180 °C. The mixing speed was set to 60 r/min. Specifically, the dried PLA, PBAT and Irganox 1076 were first mixed for 3 min, followed by the addition of BTM and mixing for another 7 min. Thereafter, MDI was added, and the mixture was continued to be compounded for 10 min. At last, the samples were obtained by hot-pressed for 10 min at 180 °C. The neat PLA/PBAT was prepared by the same procedure but without adding BTM and MDI. The crosslinked samples are coded as PLA/PBAT- *x*B/M, in which *x* represents the feeding weight ratio of BTM to the polymer matrix (PLA/PBAT). The weight ratio of PLA and PBAT is 85/15 if not specifically noted. The amount of MDI was determined by the molar ratio of the isocyanate groups to the hydroxyl group of BTM, which is controlled to be 1:1. This ratio allows the sample to have a relative high crosslinking density while still be able to relax fast due to the difficulty of complete conversion of the isocyanates in MDI.[33] The formula of the samples is listed in Table 1.

Characterizations

Fourier transform-infrared spectroscopy (FTIR) reflectance spectra were recorded on an FTIR spectrometer (Is50, Thermo Nicolet, USA) in a range of 3500–500 cm^{-1} with a resolution of 4 cm^{-1} and a scanning number of 32.

Gel permeation chromatography (GPC, Waters 1515, USA) measurements was used to get the average molecular weight (M_w) and polydispersity index (PDI). Tetrahydrofuran was used as the eluent (1 mL/min) to maintain good solubility and a polystyrene (PS) standard was used for calibration.

The gel content of the samples was estimated by measuring its insoluble part in a dried sample after placing it in a Soxhlet apparatus extracted with THF for 24 h at room temperature. The gel fraction was calculated as follows:

$$\text{Gel fraction (\%)} = W_d/W_i \times 100\% \quad (1)$$

where W_i is the initial weight of the dried sample and W_d is the weight of the dried insoluble part of the sample after Soxhlet extraction.

The melt indexes of the samples were measured according to national standard GB/T 3682-2000. The melting index is set as 190 °C and the load mass is set as 2.16 kg. The mass of the samples passing through the die port in 15 s was measured for three times, and the average value was converted into the mass of the sample passing through the die port in 10 min.

Dynamic thermomechanical analysis (DMA), heat deformation measurements, creep TTS tests were performed on a TA Q800 DMA apparatus with a rectangular sample of 10 (*l*) × 4 (*w*) × 0.5 (*t*) mm at the tensile mode. For DMA tests, the frequency and strain were set as 1 Hz and 0.1%, respectively. The scanning temperature window was −50 °C to 200 °C and the heating rate was 3 °C/min. For heat deformation measurements, the strain of the sample was recorded by heating from 40 °C to 200 °C at 5 °C/min with a stress of 0.05 MPa. Creep TTS tests were carried out from 40 °C to 75 °C in intervals of 5 °C. During the measurement of each isotherm, a constant force of 0.05 MPa was applied for 5 min followed by a 10 min recovery period.

Stress relaxation tests and frequency sweeps at high temperatures were carried out on an Anton Paar Rheometer MCR 302e under N_2 protection at a strain of 0.5% and 0.1%, relatively.

Differential scanning calorimetry (DSC) measurement was performed under a nitrogen atmosphere using a Germany 204 F1 apparatus to determine the glass transition temperatures (T_g) and melting points (T_m) of the samples. Consecutive heating-cooling-heating runs were performed under N_2 flow in a temperature window of 40 °C to 200 °C with a rate of 10 °C/min. The second heating curve was adopted for analysis.

The dumbbell-shaped splines with a length of 40 mm, a width of 4 mm, and a thickness of 0.5 mm were prepared by hot pressing the samples with a flat vulcanizer (Dongguan Kanyan Co., China). The tensile test was carried out on a universal testing machine (5967X, TW Co., American) according to the national standard GB/T 528-2009. At least 6 specimens were measured for each sample. The extension rate was set as 10 mm/min.

Morphologies of the samples were observed using a scanning electron microscope (SEM, S-4800, Japan).

The degradation behaviors of the samples were estimated in the NaOH solution (pH=13) and in compost. For the degradation behavior in NaOH solution, the weight ratio of NaOH solution to the samples was controlled to be 200:1. The samples were taken out at fixed intervals and dried in a vacuum oven before weighing. The weight loss percentage (W_L) of the samples was recorded, which was calculated as follows:

$$W_L = W_0 - W_t/W_0 \times 100\% \quad (2)$$

where W_0 and W_t are the initial weight, and the weight at different times of degradation, respectively. For the degradation behavior in compost, PLA/PBAT film samples were buried in a degradation box under constant temperature and humidity (40 °C, 60%RH). The composition of the compost degradation box is: 360 g of wood chips, 90 g of starch, 45 g of sugar, 27 g of edible oil, 18 g of urea, 270 g of rabbit food, 900 mL of deionized water, 500 g of soil, and 50 g of leaves and other corrosive substances.

Table 1 The formula of the vitrimeric PLA/PBAT blends.

Samples	PLA (g)	PBAT (g)	BTM (g)	MDI (g)	Irganox 1076 (g)
PLA/PBAT	85	15	0	0	0.3
PLA/PBAT-1B/M	85	15	1	3	0.3
PLA/PBAT-1.5B/M	85	15	1.5	4.5	0.3
PLA/PBAT-2B/M	85	15	2	6	0.3
PLA/PBAT-3B/M	85	15	3	9	0.3

https://doi.org/10.1007/s10118-023-2997-0

The shape memory behavior was investigated on a TA DMA Q800. Before deformation, the sample was heated at 90 °C and equilibrated for 5 min. First, the sample was stretched to a set stress of 0.15 MPa. Then, the sample was cooled to 25 °C at 5 °C/min before the load was removed, yielding a setting strain of ε_s. Thereafter, the stress exerted on the sample was unloaded, followed by an additional 5 min of isothermal step to ensure that the shape was fixed at 25 °C, leaving a fixed strain ε_f. At last, the sample was reheated to 90 °C at 5 °C/min to recover the strain, and the final stain was ε_r. The shape fix ratio (R_f) and shape recovery ratio (R_r) were calculated as follows:

$$R_f = \varepsilon_f/\varepsilon_s \times 100\% \quad (3)$$

$$R_r = (\varepsilon_f - \varepsilon_r)/\varepsilon_f \times 100\% \quad (4)$$

For the reconfigurable shape memory behavior, the sample was first reconfigured at 170 °C in a vacuum oven for 10 min, and then programmed at 90 °C for 2 min, and cooled at 25 °C. The final recovery process was conducted at 90 °C in hot water to conveniently take pictures or videos.

RESULTS AND DISCUSSIONS

The Network Formation

During the reactive blending process, BTM that has a tertiary amine moiety can break up and insert into PLA/PBAT chains *via* internally catalyzed transesterification, bringing in plenty of pendant or terminal hydroxyl groups to PLA or PBAT chains,[32] which can then react with MDI to form a network structure (Fig. 1). FTIR was carried out to characterize the reactions. As shown in Fig. 2(a), after adding BTM into PLA/PBAT matrix, the characteristic absorption at around 3300 cm^{-1} ascribed to the stretching vibration of —OH is observed, which is then disappeared after adding MDI. In addition, the characteristic

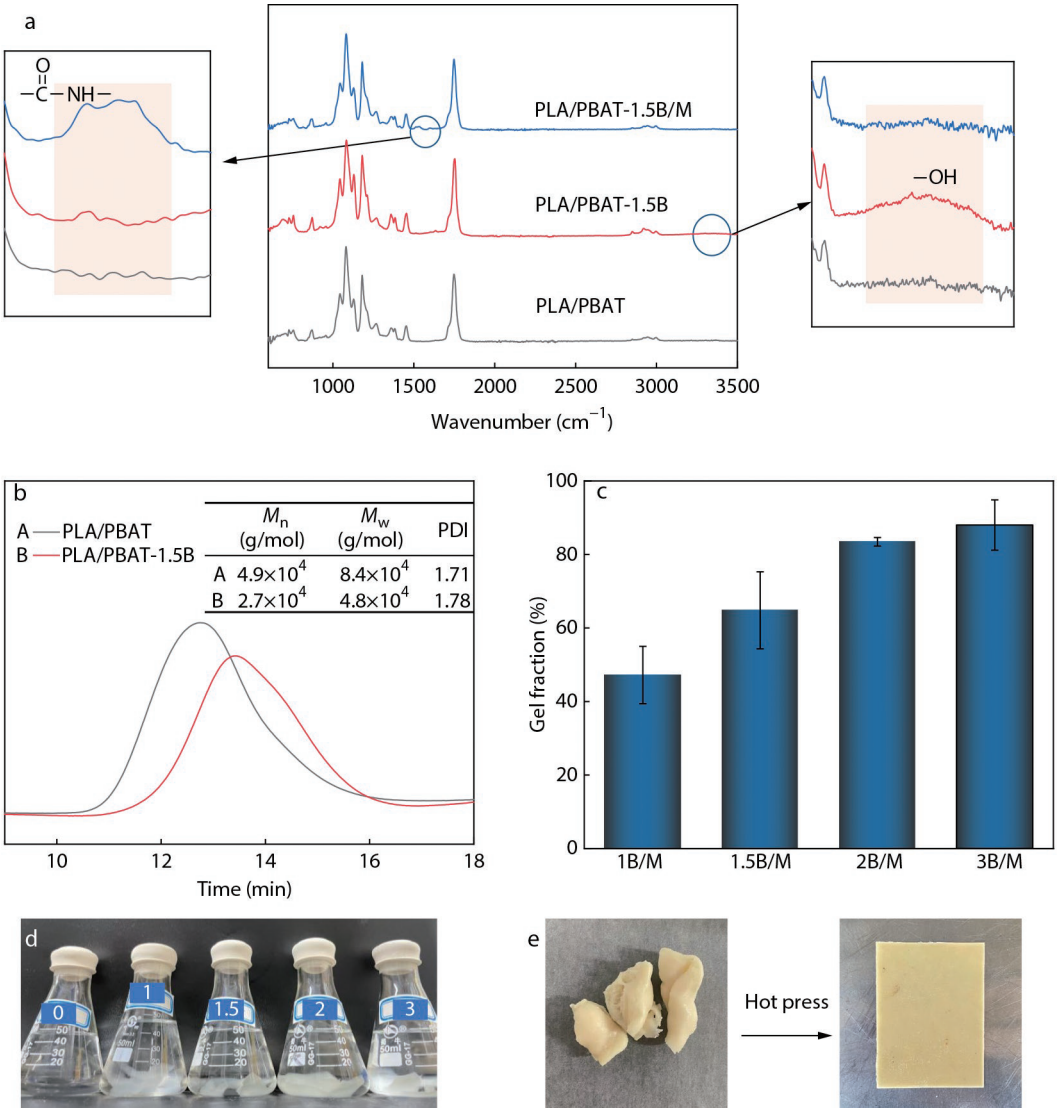

Fig. 2 (a) FTIR spectra and (b) GPC curves of PLA/PBAT, PLA/PBAT-1.5B and PLA/PBAT-1.5B/M, the inset table lists the corresponding M_n, M_w and PDI; (c) Gel fraction of the samples; (d) Photo for the samples immersed in THF for 24 h, the samples from left to right are neat PLA/PBAT and PLA/PBAT-B/M with increasing BTM amount, and (e) photos for PLA/PBAT-2B/M after reactive blending and after hot pressing.

https://doi.org/10.1007/s10118-023-2997-0

absorption at around 1530 cm^{-1} attributed to the stretching vibration of amide (II) is found after adding MDI. These results confirm the reaction between —OH and —NCO in the blends. Besides, the absence of characteristic absorption for —NCO indicates a full consumption of MDI. Moreover, the decreased molecular weight with a wider polydispersity index for the PLA/PBAT blend after adding BTM, give additional evidence to the scissor effect of BTM on the polyester chains through transesterification (Fig. 2b).[32] The network structure of PLA/PBAT-B/M is demonstrated by the increasing torque during blending, the frequency sweep at 170 °C (Figs. S1 and S2, in the electronic supplementary information, ESI) and gel fractions obtained by Soxhlet extraction using tetrahydrofuran as the solvent. As shown in Fig. 2(c), the gel fraction of the PLA/PBAT-B/M increases with increasing amounts of BTM and MDI, indicating an increased crosslinking degree. The gel fraction of PLA/PBAT-2B/M and PLA/PBAT-3B/M is higher than 80%, suggesting a well-crosslinked network. Fig. 2(d) displays the photos of the samples immersed in THF for 24 h. The PLA/PBAT-B/M was swelling while the neat PLA/PBAT was dissolved. Although PLA/PBAT-B/M were crosslinked, they are thermoplastic as demonstrated by the smooth surface of the samples after blending and hot-pressing (Fig. 2e). This is because transesterification between the residual hydroxyl groups and ester groups in the PLA or PBAT backbone occurred during reactive blending and hot pressing, leading to the rearrangement of network topology, thus endowing PLA/PBAT-B/M with vitrimeric properties.[33] These vitrimeric properties are also demonstrated by the stress relaxation behavior of PLA/PBAT-2B/M at high temperature range (170–190 °C) (Fig. S3 in ESI). However, the flowability of the PLA/PBAT-B/M is not as good as the neat PLA/PBAT blends as implied by the decreased melting index values (Fig. S4 in ESI).

Thermal Properties

The heat resistance of the blends was investigated by heat deformation curves obtained from dynamic mechanical analysis (DMA). As shown in Fig. 3(a), the strain increases with increasing temperature. An upturn beginning at around 80 °C is found for all the samples, which is attributed to the sharp decrease of the stiffness due to the glass transition of PLA. It is seen that the deformation is much slower for PLA/PBAT-B/M than neat PLA/PBAT, which indicates significantly enhanced heat resistance and dimensional stability of PLA/PBAT-B/M owning to the network structures. When the temperature rises to around 120 °C, a plateau is observed for neat PLA/PBAT and PLA/PBAT-1B/M with a low crosslinking degree. This can be ascribed to enhanced deformation resistance because of the cold crystallization of PLA, which forms a physical crosslinked

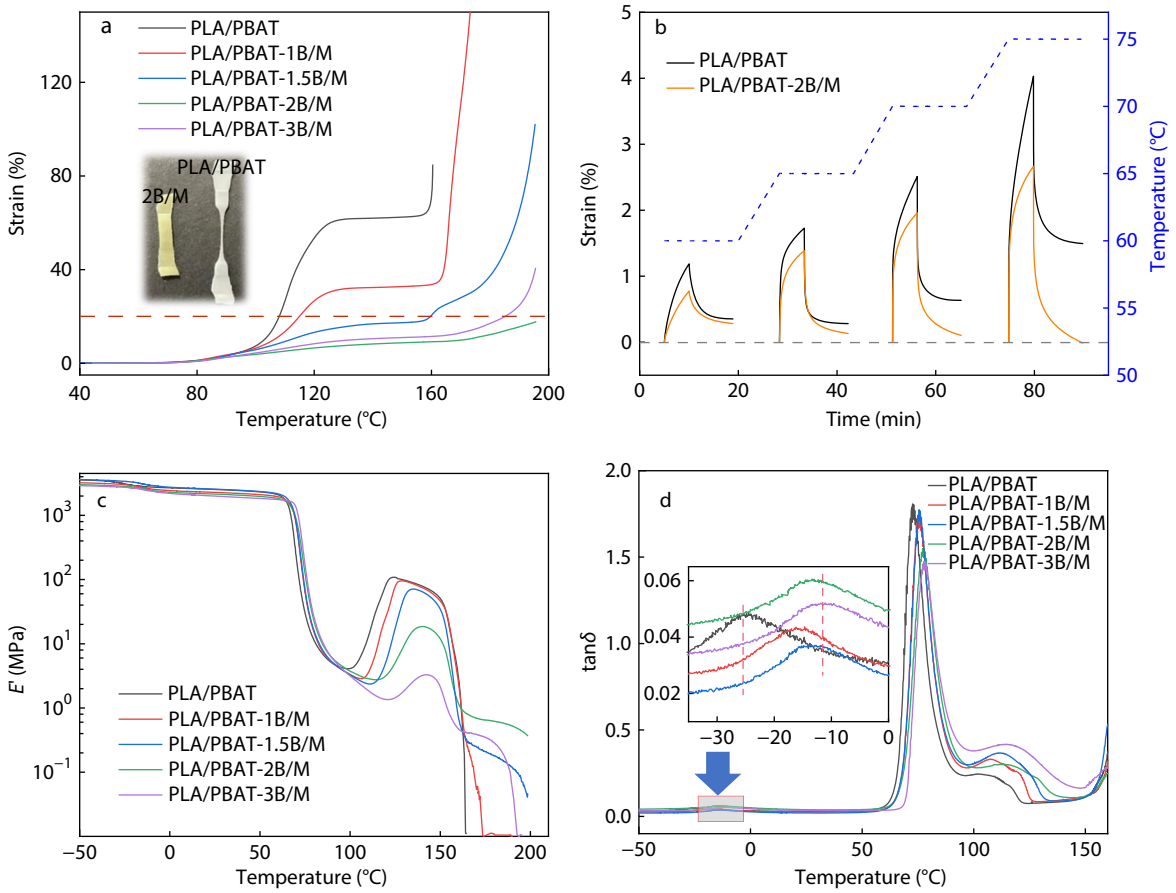

Fig. 3 (a) Heat deformation curves of neat PLA/PBAT and PLA/PBAT-B/M, the inset picture shows PLA/PBAT and PLA/PBAT-2B/M after test; (b) Creep TTS curves for PLA/PBAT and PLA/PBAT-2B/M; (c) Dependences of *E'* and (d) dependences of tan*δ* on temperature for neat PLA/PBAT and PLA/PBAT-B/M.

https://doi.org/10.1007/s10118-023-2997-0

network. As to PLA/PBAT-B/M with a higher crosslinking degree, the plateau becomes hard to distinguish, suggesting cold crystallization is suppressed due to the confined chain mobility by cross-linking, which is also manifested by the decreased melting enthalpy in DSC (Fig. S5 in ESI). Above 160 °C, the crystallization is melted, leading to a sharp strain increase for neat PLA/PBAT and PLA/PBAT-1B/M. By contrast, the strain of PLA/PBAT-B/M with a higher crosslinking degree increases much slower. However, we can still observe deformation in those samples. This can be attributed to the network rearrangement because of the exchange of hydroxyl groups and ester bonds, which is envisioned to happen above about 100 °C,[25,33] as well as the still insufficient crosslinking degree. Overall, PLA/PBAT-B/M presents much higher heat resistance and dimensional stability than neat PLA/PBAT. If we compare the temperature at 20% strain of the samples, it can be observed that the temperature at 20% strain greatly improved with increasing crosslinking degree of PLA/PBAT-B/M blends. Typically, the temperature at 20% strain of PLA/PBAT-2B/M (198 °C) is 90 °C higher than that of neat PLA/PBAT (108 °C). Moreover, as seen from the inset pictures that display the samples of neat PLA/PBAT and PLA/PBAT-2B/M after the test, PLA/PBAT-2B/M keeps its shape while neat PLA/PBAT is melted and permanently deformed. The parameters of thermal properties for the samples are listed in Table S1 (in ESI).

Additionally, creep TTS measurements for neat PLA/PBAT and PLA/PBAT-2B/M were carried out and the curves are shown in Fig. 3(b). It can be seen that the creep strain of PLA/PBAT-2B/M at different temperatures is significantly lower compared to that of neat PLA/PBAT. Besides, the recovery curve of PLA/PBAT-2B/M is convergent while that of PLA/PBAT is divergent. The creep strain of PLA/PBAT-2B/M is fully recovered at 75 °C, indicating an essential elastic deformation of PLA/PBAT-2B/M due to the cross-linked network structure. It should be mentioned that the reason that the creep recovery is not complete at lower temperatures can be the limited chain mobility resulting from insufficient glass transition. These results further illustrate that the heat resistance and dimensional stability of PLA/PBAT-B/M are significantly improved by introducing dynamic covalent crosslinks.

Figs. 3(c) and 3(d) show the dependences of storage modulus (E') and loss factor (tanδ) on temperature for neat PLA/PBAT and PLA/PBAT-B/M. With the temperature rising, E' of all the samples exhibits a sharp decrease upon glass transition, followed by an increase due to crystallization and a final decrease because of the melting of the crystals. For PLA/PBAT-B/M with a higher crosslinking degree, a plateau can be found above the melting point, suggesting an elastic network structure. It is noticed that the E' of PLA/PBAT-3B/M at the plateau region is lower than that of PLA/PBAT-2B/M. The reason for this phenomenon might be that the polymer chains were scissored too much by BTM in PLA/PBAT-3B/M, resulting in some short or branched chains that can be act as plasticizers. The crystallization of PLA/PBAT matrix is gradually suppressed with an increasing crosslinking degree, which is consistent with the above results (Fig. 3a and Fig. S5 in ESI). Because of the confinement of crosslinking points on the chain segments mobility, the glass transition temperatures (T_gs) read from tanδ curves of both PLA and PBAT are improved accompanied by decreasing peak intensity after crosslinking (Fig. 3d). Typically, compared to neat PLA/PBAT, the T_gs of PBAT and PLA in PLA/PBAT-3B/M are increased by 14 and 5 °C, respectively. These results also indicate that the crosslinking reactions occurred in both the PBAT phase and PLA phase. Notably, the T_g of the PBAT phase increases more significantly than that of the PLA phase, which may imply a higher crosslinking degree in the PBAT phase due to a possible higher reactivity of PBAT.[36] Besides, the difference between T_gs of PBAT and PLA becomes closer, suggesting better compatibility between PBAT and PLA after crosslinking. This is expectable since interfacial reactions between PBAT and PLA including transesterification and chain extension with MDI would occur during sample preparation, which greatly enhances the interfacial adhesion and reduce the interfacial tension.

Morphological Structure

The compatibility between PBAT and PLA is further revealed by the phase morphology of the blends. Fig. 4 presents the SEM images of neat PLA/PBAT and PLA/PBAT-1.5B/M. The neat PLA/PBAT displays a coarse phase-separated morphology, where spherical PBAT granules with relatively large sizes ranging from 0.5 μm to 2 μm are dispersed in the PLA matrix. In addition, extensive interfacial debonding is observed throughout the image as marked by the arrows in Figs. 4(a) and 4(c), suggesting that PBAT and PLA are poorly miscible. Concerning PLA/PBAT-1.5B/M, the size of PBAT granules is greatly decreased and the interface is blurry that is hard to distinguish, which indicates the remarkably improved compatibility and interfacial adhesion between PBAT and PLA due to the interfacial transesterification and chain extension reactions. The greatly improved compatibility between PLA and PBAT by crosslinking herein is also observed in PLA70/PBAT30-1.5B/M, which has a higher content of PBAT (the weight ratio of PLA to PBAT is 70/30), as shown in Fig. S6 (in ESI).

Mechanical Properties

The mechanical properties of the blends were studied. Fig. 5(a) presents the stress-strain curves of neat PLA, neat PLA/PBAT, and PLA/PBAT-B/M. The fracture energy that represents the

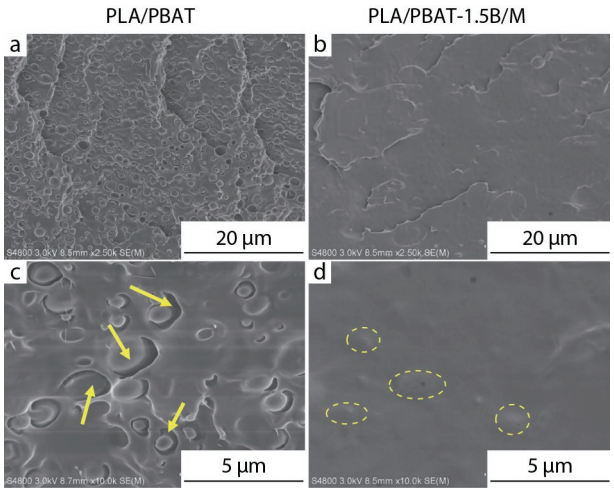

Fig. 4 SEM images of the cross-sections of (a, c) neat PLA/PBAT and (b, d) PLA/PBAT-1.5B/M.

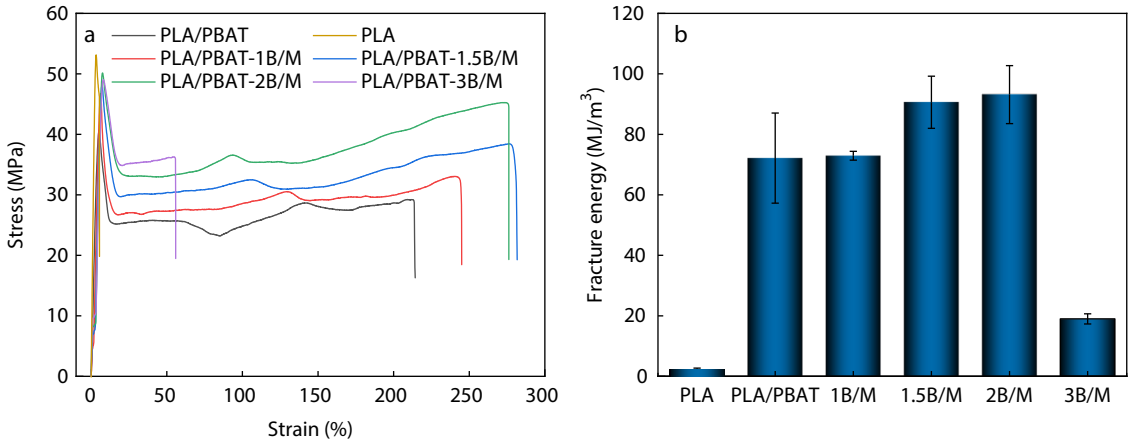

Fig. 5 (a) Stress-strain curves and (b) fracture energy for neat PLA and PLA/PBAT-B/M.

toughness of a material was calculated from the integration area of the stress-strain curves and is presented in Fig. 5(b). The related values of mechanical properties are listed in Table S2 (in ESI). From Fig. 5(a), we can see that the ductility and toughness of PLA are significantly improved after blending with PBAT (PLA/PBAT=85/15), but the tensile strengths at yielding and at break decrease obviously because of the soft nature of PBAT. After incorporating the crosslinks, both the strength and the toughness are enhanced significantly, and they increase with an increasing amount of BTM when BTM feeding ratio does not exceed 3%. The toughness is decreased for PLA/PBAT-3B/M, which may be due to the overwhelming scissors of the polymer chains and crosslinking density. Typically, the strengths at yielding and at break are improved from 45.3 MPa and 30.2 MPa (values on average, hereinafter) for neat PLA/PBAT to 50.2 MPa and 45.3 MPa for PLA/PBAT-2B/M, respectively. At the same time, the fracture energy of PLA/PBAT-2B/M is 93 MJ/m^3, which is 21 MJ/m^3 higher than that of neat PLA/PBAT. Impressively, the tensile strength at yielding and at break of PLA/PBAT-2B/M is slightly lower or comparable to those of neat PLA (53.1MPa and 46.3 MPa), yet the fracture energy is more than 40 times that for PLA, showing a good balance between strength and toughness.

A comparison of tensile strength and elongation at break for PLA/PBAT-B/M, with those of the PLA/PBAT blend reported in previous studies, is made and presented in Fig. 6. It is demonstrated that PLA/PBAT-2B/M possesses a satisfying balance between strength and toughness. The concurrent improvement of strength and toughness of PLA/PBAT-B/M can be ascribed to the synergetic contribution of the covalently crosslinked network structure and the greatly improved interfacial interactions between PLA and PBAT that promotes transfer loading. Significant improvements in the mechanical

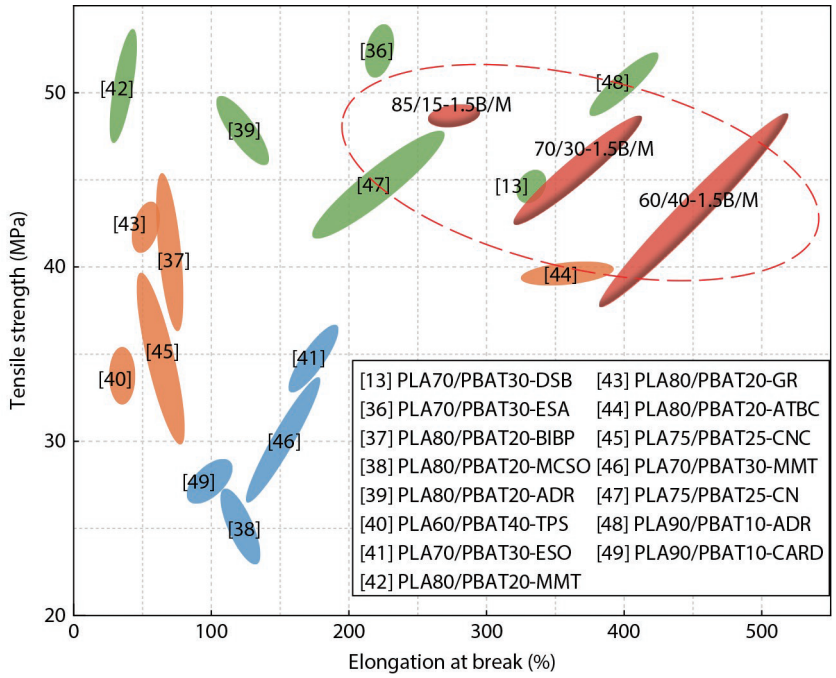

Fig. 6 Comparison of tensile strength and elongation at break for PLA/PBAT-B/M, to those of the PLA/PBAT blend reported in the literature.[13,36–49]

properties are also achieved when varying the weight ratio of PLA and PBAT (Fig. S7 in ESI). In addition, the mechanical properties of PLA/PBAT-M with only MDI but not BTM were tested to demonstrate the advantage of constructing a network over only chain extension. The tensile strength at yielding and at break of PLA/PBAT-M is significantly lower than its counterparts PLA/PBAT-1.5B/M, although the elongation at break is higher due to the plasticizing effect of excess MDI (Fig. S8 in ESI).

Shape Memory Behavior

Shape memory polymers are a kind of smart polymer materials that can memorize their temporary shape and recover the permanent shape under external stimuli, such as heat, light, pH, *etc*.[50] They have wide applications in medical care, electronic communications, aerospace, and among others. Semicrystalline PLA can be used as shape memory polymers, in which the crystalline phase and amorphous phase act as the fix phase and the reversible phase, respectively. However, very low crystallinity after regular processing and the brittle nature of PLA greatly limits its application as a shape memory polymer.[51,52] Herein, the prepared PLA/PBAT-B/M has good toughness with a network structure, thus we envisioned that it can be a good shape memory polymer. As proof of the concept, the thermally triggered shape memory behavior of neat PLA/PBAT and PLA/PBAT-2B/M was explored by DMA. As shown in Fig. 7(a), the permanent shape is deformed at 85 °C and fixed at 25 °C to yield the temporary shape, followed by a recovery by reheating to 85 °C. The fixed ratio (R_f) for both PLA/PBAT and PLA/PBAT-2B/M is as high as 100%. Owning to the good elasticity, PLA/PBAT-2B/M possesses a recovery ratio (R_r) of 93%. By contrast, R_r of PLA/PBAT is only 44%. Fig. 7(b) shows the photos for the recovery process of PLA/PBAT (white) and PLA/PBAT-2B/M (yellow) in hot water at 90 °C, which presents that the recovery of PLA/PBAT-2B/M is faster and more complete than the neat PLA/PBAT. The corresponding video is attached as Video S1 (in ESI). These results demonstrate that the PLA/PBAT-2B/M shows great potential to be used as smart shape memory polymers. Moreover, the permanent shape of PLA/PBAT-2B/M can be readily reconfigured due to its vitrimeric nature, which endows the sample with reconfigurable shape memory performance (Fig. 7c, Video S2 in ESI).

Degradation Behavior

To reveal whether the dynamic covalent network containing tertiary amine moieties influences the degradation behavior of PLA/PBAT, the degradation behavior of PLA/PBAT and PLA/PBAT-1.5B/M in NaOH solution (pH=13) (Fig. 8) and compost (Fig. S9 in ESI) were investigated. Fig. 8(a) presents the photos of the samples to visually demonstrate the change of the samples with time. The weight loss of the samples in NaOH solution was recorded and compared as shown in Fig. 8(b). It is found that PLA/PBAT-1.5B/M has a lower degradation rate compared to PLA/PBAT. Although there are tertiary amine moieties in PLA/PBAT-1.5B/M that may act as a catalyst to accelerate its degradation, the introduction of carbamate bonds that have a poorer hydrolyzing ability than the ester bonds as well as the network structure prevents the degradation of the PLA/PBAT-1.5B/M to a larger extent. However, it demonstrates a more durable nature of PLA/PBAT-B/M on the other side. How to balance the stability and the fast degradability of degradable materials in a simple way is still a big challenge.

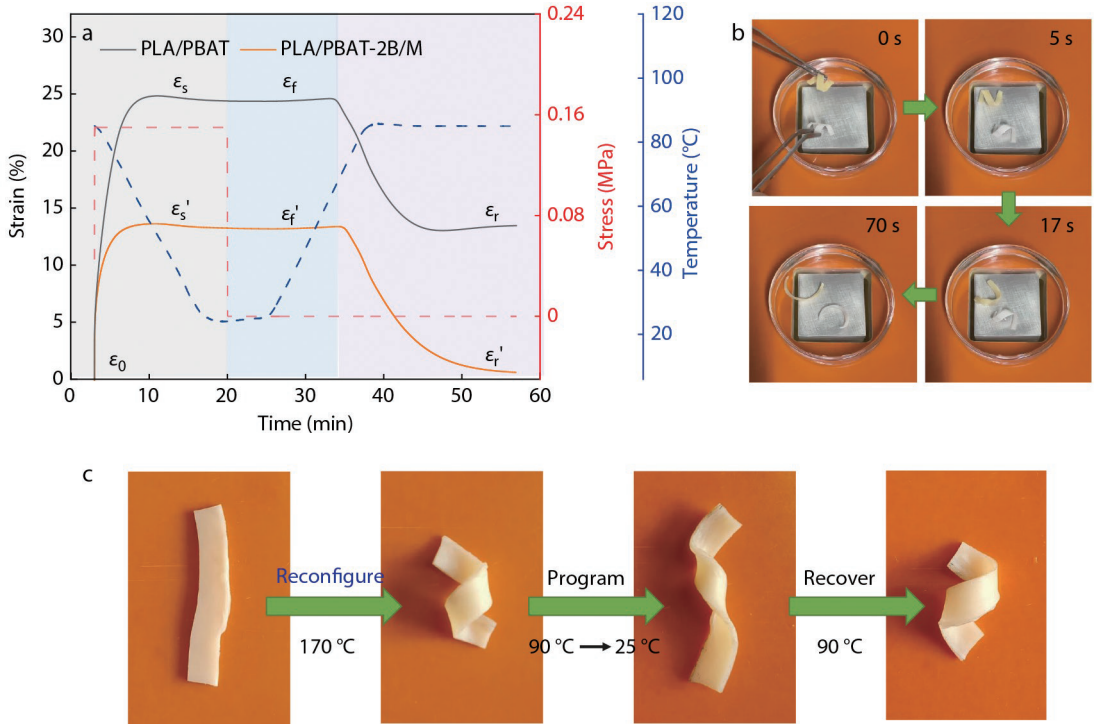

Fig. 7 (a) Shape memory program for PLA/PBAT (R_f=100%, R_r=44%) and PLA/PBAT-2B/M (R_f'=100%, R_r'=93%); (b) Photos of the recovery process of PLA/PBAT (white) and PLA/PBAT-2B/M (yellow) in hot water at 90 °C; (c) Photos of the reconfigure and program process of PLA/PBAT-2B/M.

https://doi.org/10.1007/s10118-023-2997-0

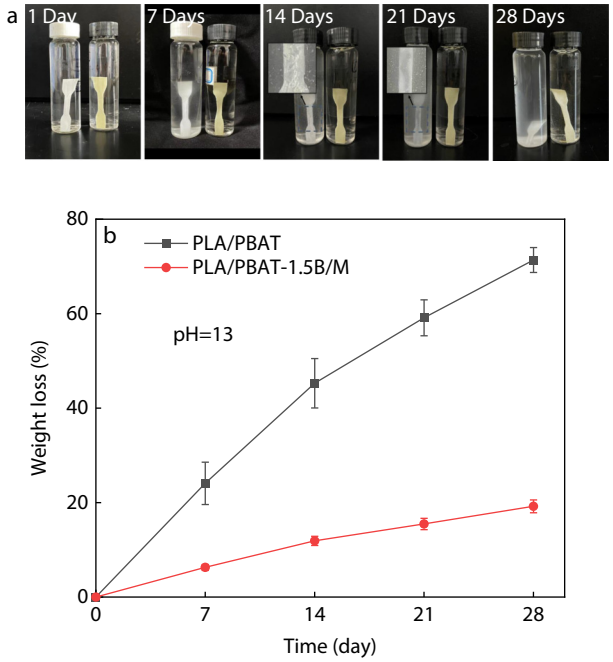

Fig. 8 Degradation behavior of PLA/PBAT and PLA/PBAT-1.5B/M immersed in NaOH solution (pH=13): (a) photos recording the change of the samples and (b) dependence of weight loss on immersing days.

CONCLUSIONS

In this study, vitrimeric PLA/PBAT blends crosslinked with exchangeable hydroxyl-ester bonds are reported, which were fabricated by straightforwardly melt-blending PLA/PBAT with a tertiary amine-containing polyol, BTM, and a diisocyanate, MDI. The network structures were confirmed by the high gel fraction above 80%. Yet, the resultant crosslinked blends can be processed by reactive blending and hot pressing due to their vitrimeric nature endowed by the exchangeable hydroxyl-ester bonds. Attributed to the network structure, the heat resistance of the blends is greatly enhanced. Typically, the temperature at 20% increases by 80 °C for PLA/PBAT-2B/M, and the sample can keep its shape after heating to 200 °C. In addition, the interfacial compatibility and adhesion between PLA and PBAT are remarkably improved ascribed to interfacial transesterification and chain extension reactions. This further leads to significantly improving in both the tensile strength and toughness of the blend. PLA/PBAT-2B/M possesses a tensile strength of 50.2 MPa and a fracture energy of 93 MJ/m^3, which exhibits a good balance between strength and toughness. Furthermore, the resultant PLA/PBAT blends show promising reconfigurable shape memory behavior with good recovery. This work offers a promising approach to fabricating high-performance and functional PLA/PBAT blends, which is envisioned to be readily extended to other fully biodegradable polyester blends.

Conflict of Interests

The authors declare no interest conflict.

Electronic Supplementary Information

Electronic supplementary information (ESI) is available free of charge in the online version of this article at http://doi.org/10.1007/s10118-023-2997-0.

ACKNOWLEDGMENTS

This work was financially supported by the National Natural Science Foundation of China (Nos. 21975108 and 52103082), Fundamental Research Funds for the Central Universities (No. JUSRP122016), Wuxi "Light of Taihu Lake" Science and Technology Research Plan (Basic Research, No. K20221008).

REFERENCES

1 Chemistry can help make plastics sustainable - but it isn't the whole solution. *Nature* **2021**, *590*, 363–364.
2 Silva, A. L. P.; Prata, J. C.; Walker, T. R.; Duarte, A. C.; Ouyang, W.; Barcelo, D.; Rocha-Santos, T. Increased plastic pollution due to Covid-19 pandemic: challenges and recommendations. *Chem. Eng. J.* **2021**, *405*, 126683.
3 Flury, M.; Narayan, R. Biodegradable plastic as an integral part of the solution to plastic waste pollution of the environment. *Curr. Opin. Green Sustain. Chem.* **2021**, *30*, 2452–2236.
4 Ghosh, K.; Jones, B. H. Roadmap to biodegradable plastics—current state and research needs. *ACS Sustainable Chem. Eng.* **2021**, *9*, 6170–6187.
5 Altman, R. The myth of historical bio-based plastics early bio-based plastics, which were neither clean nor green, offer lessons for today. *Science* **2021**, *373*, 47–49.
6 Farah, S.; Anderson, D. G.; Langer, R. Physical and mechanical properties of PLA, and their functions in widespread applications—a comprehensive review. *Adv. Drug Deliv. Rev.* **2016**, *107*, 367–392.
7 Tripathi, N.; Misra, M.; Mohanty, A. K. Durable polylactic acid (PLA)-based sustainable engineered blends and biocomposites: recent developments, challenges, and opportunities. *ACS Eng. Au* **2021**, *1*, 7–38.
8 Yeo, J. C. C.; Muiruri, J. K.; Koh, J. J.; Thitsartarn, W.; Zhang, X. K.; Kong, J. H.; Lin, T. T.; Li, Z. B.; He, C. B. Bend, twist, and turn: first bendable and malleable toughened PLA green composites. *Adv. Funct. Mater.* **2020**, *30*, 2001565.
9 Qu, Y. D.; Chen, Y. H.; Ling, X. Y.; Wu, J. L.; Hong, J. T.; Wang, H. T.; Li, Y. J. Reactive micro-crosslinked elastomer for supertoughened polylactide. *Macromolecules* **2022**, *55*, 7711–7723.
10 Dong, X. Y.; Wu, Z. G.; Wang, Y.; Li, T.; Yuan, H.; Zhang, X. H.; Ma, P. M.; Chen, M. Q.; Dong, W. F. Design of degradable core-shell starch nanoparticles by radical ring-opening polymerization of 2-methylene-1,3-dioxepane and their toughening of poly(lactic acid). *Compos. Commun.* **2021**, *27*, 100808.
11 Hamad, K.; Kaseem, M.; Ayyoob, M.; Joo, J.; Deri, F. Polylactic acid blends: the future of green, light and tough. *Prog. Polym. Sci.* **2018**, *85*, 83–127.
12 Yang, H. R.; Jia, G.; Wu, H.; Ye, C. C.; Yuan, K.; Liu, S. L.; Zhou, L. M.; Xu, H.; Gao, L. J.; Cui, J.; Fang, S. M. Design of fully biodegradable super-toughened PLA/PBAT blends with asymmetric composition *via* reactive compatibilization and controlling morphology. *Mater. Lett.* **2022**, *329*, 133067.
13 Chen, J. L.; Rong, C. Y.; Lin, T. T.; Chen, Y. H.; Wu, J. L.; You, J. C.; Wang, H. T.; Li, Y. J. Stable co-continuous PLA/PBAT blends compatibilized by interfacial stereocomplex crystallites: toward

full biodegradable polymer blends with simultaneously enhanced mechanical properties and crystallization rates. *Macromolecules* **2021**, *54*, 2852–2861.
14 Mohammadi, M.; Bruel, C.; Heuzey, M. C.; Carreau, P. J. CNC dispersion in PLA and PBAT using two solvents: morphological and rheological properties. *Cellulose* **2020**, *27*, 9877–9892.
15 Dong, X. Y.; Liu, L.; Wang, Y.; Li, T.; Wu, Z. G.; Yuan, H.; Ma, P. M.; Shi, D. J.; Chen, M. Q.; Dong, W. F. The compatibilization of poly(propylene carbonate)/poly(lactic acid) blends in presence of core-shell starch nanoparticles. *Carbohydr. Polym.* **2021**, *254*, 8.
16 Cvek, M.; Paul, U. C.; Zia, J.; Mancini, G.; Sedlarik, V.; Athanassiou, A. Biodegradable films of PLA/PPC and curcumin as packaging materials and smart indicators of food spoilage. *ACS Appl. Mater. Interfaces* **2022**, *14*, 14654–14667.
17 Mulchandani, N.; Masutani, K.; Kumar, S.; Yamane, H.; Sakurai, S.; Kimura, Y.; Katiyar, V. Toughened PLA-*b*-PCL-*b*-PLA triblock copolymer based biomaterials: effect of self-assembled nanostructure and stereocomplexation on the mechanical properties. *Polym. Chem.* **2021**, *12*, 3806–3824.
18 Zhang, C. M.; Zhai, T. L.; Turng, L. S.; Dan, Y. Morphological, mechanical, and crystallization behavior of polylactide/polycaprolactone blends compatibilized by L-lactide/caprolactone copolymer. *Ind. Eng. Chem. Res.* **2015**, *54*, 9505–9511.
19 Vidhya Nagarajan, K. Z., Manjusri Misra, Amar K. Mohanty. Overcoming the fundamental challenges in improving the impact strength and crystallinity of PLA biocomposites: influence of nucleating agent and mold temperature. *ACS Appl. Mater. Interfaces* **2015**, *7*, 11203–11214.
20 Si, W. J.; Zhang, H.; Li, Y. D.; Huang, C. L.; Weng, Y. X.; Zeng, J. B. Highly toughened and heat resistant poly(L-lactide)/poly(ε-caprolactone) blends *via* engineering balance between kinetics and thermodynamics of phasic morphology with stereocomplex crystallite. *Compos. B Eng.* **2020**, *197*, 1359–8368.
21 Zhao, X. P.; Liu, J. C.; Li, J. C.; Liang, X. Y.; Zhou, W. Y.; Peng, S. X. Strategies and techniques for improving heat resistance and mechanical performances of poly(lactic acid) (PLA) biodegradable materials. *Int. J. Biol. Macromol.* **2022**, *218*, 115–134.
22 Bednarek, M.; Borska, K.; Kubisa, P. New polylactide-based materials by chemical crosslinking of PLA. *Polym. Rev.* **2021**, *61*, 493–519.
23 Tillet, G.; Boutevin, B.; Ameduri, B. Chemical reactions of polymer crosslinking and post-crosslinking at room and medium temperature. *Prog. Polym. Sci.* **2011**, *36*, 191–217.
24 Nagasawa, N.; Kasai, N.; Yagi, T.; Yoshii, F.; Tamada, M. Radiation-induced crosslinking and post-processing of poly(L-lactic acid) composite. *Radiat. Phys. Chem.* **2011**, *80*, 145–148.
25 Montarnal, D.; Capelot, M.; Tournilhac, F.; Leibler, L. Silica-like malleable materials from permanent organic networks. *Science* **2011**, *334*, 965–968.
26 Van Zee, N. J.; Nicolay, R. Vitrimers: permanently crosslinked polymers with dynamic network topology. *Prog. Polym. Sci.* **2020**, *104*, 67–79.
27 Rottger, M.; Domenech, T.; van der Weegen, R.; Nicolay, A. B. R.; Leibler, L. High-performance vitrimers from commodity thermoplastics through dioxaborolane metathesis. *Science* **2017**, *356*, 62–65.
28 Lessard, J. J.; Garcia, L. F.; Easterling, C. P.; Sims, M. B.; Bentz, K. C.; Arencibia, S.; Savin, D. A.; Sumerlin, B. S. Catalyst-free vitrimers from vinyl polymers. *Macromolecules* **2019**, *52*, 2105–2111.
29 Wang, S.; Ma, S. Q.; Qiu, J. F.; Tian, A. P.; Li, Q.; Xu, X. W.; Wang, B. B.; Lu, N.; Liu, Y. L.; Zhu, J. Upcycling of post-consumer polyolefin plastics to covalent adaptable networks *via in situ* continuous extrusion cross-linking. *Green Chem.* **2021**, *23*, 2931–2937.
30 Saed, M. O.; Lin, X. Y.; Terentjev, E. M. Dynamic semicrystalline networks of polypropylene with thiol-anhydride exchangeable crosslinks. *ACS Appl. Mater. Interfaces* **2021**, *13*, 42055–42062.
31 Demongeot, A.; Groote, R.; Goossens, H.; Hoeks, T.; Tournilhac, F.; Leibler, L. Cross-linking of poly(butylene terephthalate) by reactive extrusion using Zn(II) epoxy-vitrimer chemistry. *Macromolecules* **2017**, *50*, 6117–6127.
32 Qiu, J. F.; Ma, S. Q.; Wang, S.; Tang, Z. B.; Li, Q.; Tian, A. P.; Xu, X. W.; Wang, B. B.; Lu, N.; Zhu, J. Upcycling of polyethylene terephthalate to continuously reprocessable vitrimers through reactive extrusion. *Macromolecules* **2021**, *54*, 703–712.
33 Brutman, J. P.; Delgado, P. A.; Hillmyer, M. A. Polylactide vitrimers. *ACS Macro Lett.* **2014**, *3*, 607–610.
34 Borska, K.; Bednarek, M.; Pawlak, A. Reprocessable polylactide-based networks containing urethane and disulfide linkages. *Eur. Polym. J.* **2021**, *156*, 0014–3057.
35 Liu, Y. B.; Peng, L. M.; Bao, R. Y.; Yang, M. B.; Yang, W. Vitrimeric polylactide by two-step alcoholysis and transesterification during reactive processing for enhanced melt strength. *ACS Appl. Mater. Interfaces* **2022**, *14*, 45966–45977.
36 Chen, X.; Zeng, Z.; Ju, Y.; Zhou, M.; Bai, H.; Fu, Q. Design of biodegradable PLA/PBAT blends with balanced toughness and strength *via* interfacial compatibilization and dynamic vulcanization. *Polymer* **2023**, *266*, 125620.
37 Ai, X.; Li, X.; Yu, Y. L.; Pan, H. W.; Yang, J.; Wang, D. M.; Yang, H. L.; Zhang, H. L.; Dong, L. S. The mechanical, thermal, rheological and morphological properties of PLA/PBAT blown films by using bis(tert-butyl dioxy isopropyl) benzene as crosslinking agent. *Polym. Eng. Sci.* **2019**, *59*, E227–E236.
38 Carbonell-Verdu, A.; Ferri, J. M.; Dominici, F.; Boronat, T.; Sanchez-Nacher, L.; Balart, R.; Torre, L. Manufacturing and compatibilization of PLA/PBAT binary blends by cottonseed oil-based derivatives. *Express Polym. Lett.* **2018**, *12*, 808–823.
39 da Silva, J. M. F.; Soares, B. G. Epoxidized cardanol-based prepolymer as promising biobased compatibilizing agent for PLA/PBAT blends. *Polym. Test.* **2021**, *93*, 7.
40 Qi, J.; Pan, Y. T.; Luo, Z. L.; Wang, B. B. Facile and scalable fabrication of bioderived flame retardant based on adenine for enhancing fire safety of fully biodegradable PLA/PBAT/TPS ternary blends. *J. Appl. Polym. Sci.* **2021**, *138*, 17.
41 Han, Y.; Shi, J. W.; Mao, L. X.; Wang, Z.; Zhang, L. Q. Improvement of compatibility and mechanical performances of PLA/PBAT composites with epoxidized soybean oil as compatibilizer. *Ind. Eng. Chem. Res.* **2020**, *59*, 21779–21790.
42 Ludwiczak, J.; Frackowiak, S.; Leluk, K. Study of thermal, mechanical and barrier properties of biodegradable PLA/PBAT films with highly oriented MMT. *Materials* **2021**, *14*, 12.
43 Aldas, M.; Ferri, J. M.; Motoc, D. L.; Peponi, L.; Arrieta, M. P.; Lopez-Martinez, J. Gum rosin as a size control agent of poly(butylene adipate-*co*-terephthalate) (PBAT) domains to increase the toughness of packaging formulations based on polylactic acid (PLA). *Polymers* **2021**, *13*, 19.
44 Aliotta, L.; Canesi, I.; Lazzeri, A. Study on the preferential distribution of acetyl tributyl citrate in poly (lactic) acid-poly(butylene adipate-*co*-terephthalate) blends. *Polym. Test.* **2021**, *98*, 14.
45 Sarul, D. S.; Arslan, D.; Vatansever, E.; Kahraman, Y.; Durmus, A.; Salehiyan, R.; Nofar, M. Preparation and characterization of PLA/PBAT/CNC blend nanocomposites. *Colloid. Polym. Sci.* **2021**, *299*, 987–998.
46 He, H. Z.; Liu, B. D.; Xue, B.; Zhang, H. Study on structure and properties of biodegradable PLA/PBAT/organic-modified MMT nanocomposites. *J. Thermoplast. Compos. Mater.* **2022**, *35*,

503–520.
47 Nofar, M.; Salehiyan, R.; Ciftci, U.; Jalali, A.; Durmus, A. Ductility improvements of PLA-based binary and ternary blends with controlled morphology using PBAT, PBSA, and nanoclay. *Compos. B Eng.* **2020**, *182*, 13.
48 Wang, X.; Peng, S. X.; Chen, H.; Yu, X. L.; Zhao, X. P. Mechanical properties, rheological behaviors, and phase morphologies of high-toughness PLA/PBAT blends by *in-situ* reactive compatibilization. *Compos. B. Eng.* **2019**, *173*, 10.
49 Thiyagu, T. T.; Kumar, J.; Gurusamy, P.; Sathiyamoorthy, V.; Maridurai, T.; Prakash, V. R. A. Effect of cashew shell biomass synthesized cardanol oil green compatibilizer on flexibility, barrier, thermal, and wettability of PLA/PBAT biocomposite films. *Biomass Convers. Biorefin.* **2021**, *23*, 11.
50 Zheng, N.; Fang, Z. Z.; Zou, W. K.; Zhao, Q.; Xie, T. Thermoset shape-memory polyurethane with intrinsic plasticity enabled by transcarbamoylation. *Angew. Chem. Int. Ed.* **2016**, *55*, 11421–11425.
51 Cao, L. M.; Liu, C.; Zou, D. J.; Zhang, S. D.; Chen, Y. K. Using cellulose nanocrystals as sustainable additive to enhance mechanical and shape memory properties of PLA/ENR thermoplastic vulcanizates. *Carbohydr. Polym.* **2020**, *230*, 8.
52 He, S. Y.; Hu, S. K.; Wu, Y. W.; Jin, R. H.; Niu, Z. H.; Wang, R. G.; Xue, J. J.; Wu, S. Z.; Zhao, X. Y.; Zhang, L. Q. Polyurethanes based on polylactic acid for 3D printing and shape-memory applications. *Biomacromolecules* **2022**, *34*, 11.

https://doi.org/10.1007/s10118-023-2997-0